Sedimentary Geology 437 (2022) 106180

Contents lists available at ScienceDirect

Sedimentary Geology

journal homepage: www.elsevier.com/locate/sedgeo

Million-year-scale changes in the provenance of the Miocene Doumsan fan-delta system, Pohang Basin, SE Korea: Separating the effects of eustasy and tectonic subsidence

Hyojong Lee [a], Jeong-Hyun Lee [b,c,*], Taejin Choi [d], Min-Kyu Oh [c], Sung Hi Choi [b,c]

[a] Korea Institute of Geoscience and Mineral Resources, Daejeon 34132, Republic of Korea
[b] Department of Geological Sciences, Chungnam National University, Daejeon 34134, Republic of Korea
[c] Department of Astronomy, Space Science and Geology, Chungnam National University, Daejeon 34134, Republic of Korea
[d] Department of Earth Science Education, Korea National University of Education, Cheongju 28173, Republic of Korea

ARTICLE INFO

Article history:
Received 12 April 2022
Received in revised form 26 May 2022
Accepted 30 May 2022
Available online 02 June 2022

Editor: Dr. Catherine Chagué

Keywords:
Fan delta
Drainage basin
Detrital zircon
Miocene
Whole-rock geochemistry

ABSTRACT

The relationships between fan deltas and their drainage basins have been extensively studied for the present day, but as far as we are aware of, studies have not yet been performed for the geologic record. This study examines the provenance of the Miocene Doumsan fan-delta system (17–10.5 Ma), Pohang Basin, southeast Korea, using combined detrital zircon and whole-rock geochemistry to understand the long-term development of the fan-delta system and its drainage basin. Of the lower five sequences of the Doumsan fan-delta, which were interpreted to have been controlled solely by eustasy, the lower sequences (sequences 1–3) show gradual expansion of the drainage basin without tectonic activity. In contrast, sequence 4 records an abrupt shrinkage of the drainage basin induced by uplift of the source area at ca. 15 Ma, which could have resulted from a regional collisional tectonic event that has not yet been recognised from the fan delta systems of the Pohang Basin, although palaeomagnetic studies and compositional changes of basalts of the basin suggest this event. Sequence 5 records a subsequent gradual expansion of the source area during tectonic quiescence. Warm and humid climatic conditions in East Asia during the middle Miocene would have resulted in a relatively large drainage basin. This study thus demonstrates how eustasy and tectonic subsidence as well as climate can control the drainage basins of fan-delta systems over timescales of several million years.

1. Introduction

Upland catchments (i.e., drainage basins) export sediments to the adjacent lowlands like "a well-directed fire hose" (Allen, 2008). In proximal depositional environments, coarse-grained sediments originating from a drainage basin can accumulate as an alluvial fan. Extensive studies of modern fans have demonstrated that there is a positive relationship between the size of the drainage basin and that of the associated fan (e.g., Bull, 1977; Harvey, 1989; Blair and McPherson, 2009). Tectonic uplift and climate changes in the source area may control the relationship because these factors can easily modify the sediment supply rate from the source area (e.g., Allen and Hovius, 1998; Allen and Densmore, 2000; Densmore et al., 2007). Tectonically induced basin subsidence or eustatic sea-level changes may determine the vertical sediment accumulation rate in fan areas (e.g., Whipple and Trayler, 1996; Calvache et al., 1997; Harvey et al., 1999). Most previous studies of these relationships, however, have been limited to research on modern fans or model simulations (e.g., Tucker and Whipple, 2002; Crosta and Frattini, 2004; Densmore et al., 2007), hindering our understanding of the sequential development of a fan-delta system and its drainage basin.

Miocene fan deltas are well recognised in the Pohang Basin, which is a wedge-shaped pull-apart basin in southeast Korea (Han et al., 1987; Kim, 1992; Yoon and Chough, 1995; Sohn et al., 2001; Sohn and Son, 2004; Son et al., 2013, 2015). The basin formed during back-arc opening of the East Sea (Sea of Japan) between the Korean Peninsula and the Japanese Islands. Normal faults with throws of more than a kilometre formed at the western margin of the basin, where several fan-delta systems consequently developed (Chough et al., 1990; Hwang and Chough, 1990; Hwang et al., 1995; Hong et al., 1998; Sohn et al., 2001; Sohn and Son, 2004). Of these systems, the Doumsan fan-delta system is the largest, with a radius of >8 km (Chough et al., 1990; Hwang et al., 1995; Sohn et al., 2001). Sequence stratigraphic study of the fan-delta succession has suggested that the fan-delta development was solely

* Corresponding author at: Department of Geological Sciences, Chungnam National University, Daejeon 34134, Republic of Korea.
E-mail address: jeonghyunlee@cnu.ac.kr (J.-H. Lee).

https://doi.org/10.1016/j.sedgeo.2022.106180
0037-0738/

controlled by eustatic sea-level rise and fall during the middle Miocene (about 17–10.5 Ma) after initial downfaulting of the normal fault at ca. 17 Ma (Sohn et al., 2001).

In this study, we examine the drainage basin development of the Doumsan fan-delta system using combined detrital zircon U–Pb dating and whole-rock geochemistry, and discuss their implications. Variations in the lithology of the source area enable us to infer the evolution of the drainage area through changes in sediment provenance. Contrary to the previous conclusion that development of the fan-delta system was controlled solely by eustasy (Sohn et al., 2001), we reveal that major tectonic subsidence affected the fan development at ca. 15 Ma, coinciding with a previously known tectonic event that affected the adjacent Tsushima Island (Son et al., 2015) and Japan (e.g., Jolivet and Tamaki, 1992; Fabbri et al., 1996; Itoh, 2001) as well as the Pohang Basin (Moon et al., 2000; Choi et al., 2013; Son et al., 2013, 2015). The results of this study improve our understanding of the tectonic development of the Pohang Basin and constitute an excellent example of million-year-scale changes in a fan delta and its drainage basin.

2. Geological setting

Back-arc opening of the East Sea caused crustal deformation in the southeastern Korean Peninsula and nearby areas during the Miocene, resulting in the formation of several pull-apart extensional sedimentary basins along the southeast coast of Korea (Son et al., 2013, 2015). The Pohang Basin is the largest Miocene sedimentary basin in the area (Fig. 1a), and it is filled with a ~1-km-thick sequence of nonmarine to marine sedimentary rocks comprising conglomerate, sandstone, and mudstone (Um et al., 1964; Hwang et al., 2021). The western margin is bounded by a NNE-striking zigzag-shaped fault zone that is composed of small segments of NNE-striking normal faults and NW-striking transfer faults (Sohn and Son, 2004; Son et al., 2013, 2015). The southern to southeastern margins are bounded by the Ocheon Fault system (Cheon et al., 2012). The northern to eastern margins are not clearly defined because they are submerged in the East Sea. Palaeontological studies have suggested that deposition in the Pohang Basin initiated before 17 Ma and continued until ca. 10 Ma (Kim, 1990; Yi and Yun, 1995).

2.1. Fan delta system

During the development of the Pohang Basin, the western fault zone acted as a major normal fault (Hong et al., 1998; Son et al., 2015). Sediments were eroded from the western areas over the fault zone and transported to the east, forming six fan-delta systems along the fault zone, which are the Yugye, Gohyun, Duksung, Maesan, Doumsan, and Malgol fan deltas from north to south (Fig. 1b) (Hwang et al., 1995; Hong et al., 1998). In the present day, most of the fan-delta deposits strike north and dip ~10° to the east (Um et al., 1964).

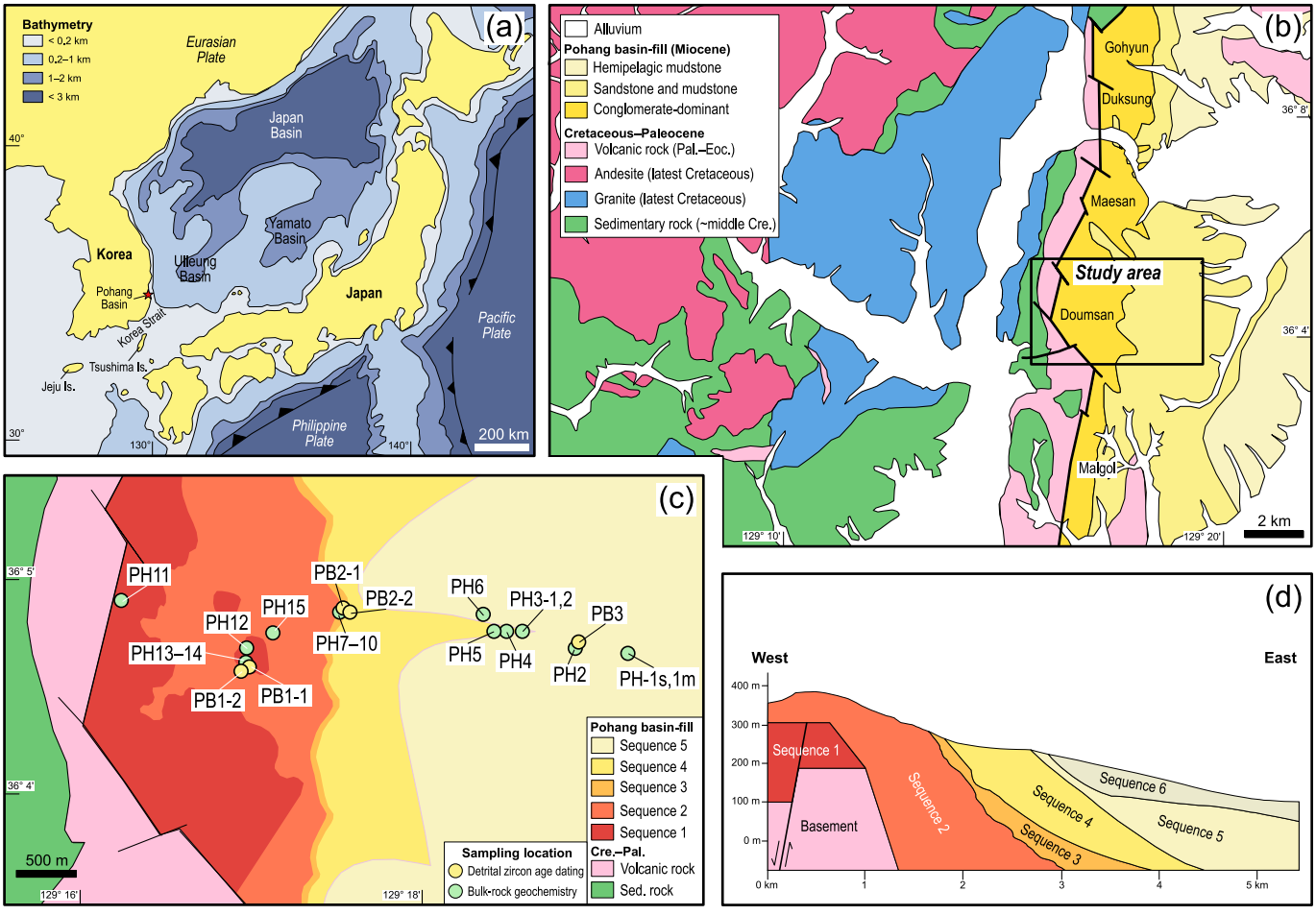

Fig. 1. (a) Location and physiography of the Pohang Basin shown on the regional tectonic map (modified from Ingle, 1992). (b) Geological map of the Pohang basin-fill and the western source area (modified from Um et al., 1964; Oh and Jeong, 1975; Hwang et al., 1995; Hong et al., 1998). (c) Geological map of the Doumsan fan-delta deposits (modified from Hwang et al., 1995; Sohn et al., 2001). The Doumsan fan-delta deposits can be subdivided into six depositional sequences bounded by regional erosional surfaces (Sohn et al., 2001). Samples were collected from sequences 1 to 5 (for sample lithology and locations, see Supplementary Table 1). (d) Cross-section of the Doumsan fan delta (modified after Sohn et al., 2001, fig. 13). Abbreviations: Cre., Cretaceous; Eoc., Eocene; Pal., Paleocene; Sed., Sedimentary.

The sedimentological formation and development of the Doumsan fan-delta system, the largest fan delta in the Pohang Basin (>8 km radius), has been investigated extensively (Chough et al., 1990; Hwang, 1993; Hwang et al., 1995; Sohn et al., 1997, 2001). In the earliest stage, the Doumsan fan-delta system developed as a small alluvial fan prograding eastward into a shallow-marine environment. Major downfaulting occurred at ca. 17 Ma, resulting in a rapid rise of relative sea-level and deposition of conglomerate deposits as Gilbert-type fan-delta foresets. Tectonism might have subsequently diminished, resulting in deposition of fine-grained sedimentary rocks (mainly sandstones and hemipelagic mudstones), with an overall transition of depositional environment from Gilbert-type foreset, to prodelta, to slope-apron, to basin plain (Hwang et al., 1995). Based on the occurrence of regional stratigraphic discontinuities (erosional surfaces), Sohn et al. (2001) re-interpreted the development of the Doumsan fan-delta systems under a sequence stratigraphic framework, and subdivided the fan-delta deposits into six depositional sequences (Fig. 1d). Sohn et al. (2001) named the lowest transgressive succession (a transition from alluvial-fan to shallow marine deposits) and the Gilbert type fan-delta foresets sequences 1 and 2, respectively. The rest of the sequences (sequences 3–6) consist of alternating lower submarine conglomerate and upper hemipelagic mudstone. Sohn et al. (2001) proposed that the development of sequences 1 and 2 was controlled by back-arc opening of the East Sea (ca. 17 Ma); sequence 1 was formed by gradual subsidence prior to 17 Ma, and sequence 2 resulted from abrupt downfaulting of the Pohang region ~17 Ma. In contrast, development of sequences 3–6 was interpreted to have been primarily controlled by third-order eustatic sea-level cycles rather than regional tectonism (Sohn et al., 2001). In this view, these upper sequences have erosional surfaces at their base that formed during eustatic sea-level fall, followed by successive lowstand (conglomerate) and highstand (mudstone) deposits formed during sea-level rise (Sohn et al., 2001).

2.2. Source area geology

Along the western fault zone, felsic volcanic rocks and sedimentary rocks occur as a narrow belt (<1 km wide), unconformably underlying the Pohang Basin fills (Um et al., 1964; Oh and Jeong, 1975; Hwang et al., 1995; Hong et al., 1998). The sedimentary rocks are nonmarine siliciclastic deposits composed of sandstone, siltstone, and reddish or dark grey mudstone, and they extend broadly to the southwest. A large mass of granitic rock composed of biotite granite and granodiorite is also exposed near the western fault zone. The granitic rocks extend up to 10 km from the western fault zone. An andesite mass is exposed adjacent to the west side of the granitic rock body, covering a large area up to 30 km from the western fault zone.

The sedimentary rocks are the oldest rocks in the western source area of the Pohang Basin. They are considered to be equivalent to the Hayang Group of the Cretaceous Gyeongsang Basin fills (Um et al., 1964; Oh and Jeong, 1975). The depositional age of the Cretaceous rocks has been approximately restricted to the middle Cretaceous based on U—Pb detrital zircon and K—Ar whole-rock age dating (Paik et al., 2012 and references therein). Previous provenance studies have reported that the Hayang Group contains mainly Palaeoproterozoic, Triassic–Jurassic, and middle Cretaceous zircons, with the youngest zircon ages being Cenomanian to Aptian (Lee et al., 2018; Choi and Kwon, 2019).

After deposition of the Cretaceous sedimentary rocks, magmatism occurred from the Late Cretaceous to early Eocene in the southwestern Korean Peninsula (Kim et al., 2016; Hwang et al., 2019b), causing intrusion and extrusion of igneous rocks in the western source areas of the Doumsan fan-delta system. In early geological surveys near the study area, felsic volcanic rocks were considered to have formed during the Cretaceous, with granitic rocks and andesite (Um et al., 1964; Oh and Jeong, 1975). In more recent studies, however, it has been revealed that granitic rocks and andesite formed mainly during the early stage of magmatism, and the felsic volcanic rocks that overlie the granitic rocks and andesite formed later (e.g., Jin et al., 1988; Hwang, 2002, 2017). The age of the granitic rocks in the study area has not been determined, but similar rocks in the adjacent area formed at 77–76 Ma (Cheongsong area; Hwang et al., 2016, 2017) and 72–71 Ma (Eonyang–Yangsan area; Zhang et al., 2012), suggesting that their intrusion occurred in the latest Cretaceous (Cheong and Kim, 2012). The andesite is also considered to have formed during the latest Cretaceous, although its exact eruption age has not yet been clearly reported (Hwang, 2002, 2017; Hwang et al., 2019a). Felsic volcanic eruptions might have initiated from the latest Cretaceous, but mostly occurred through the Paleocene and earliest Eocene (66–49 Ma; Jin et al., 1988; Jin et al., 1989; Shin, 2013; Lee et al., 2014; Hwang, 2017; Hwang et al., 2019a).

3. Analytical methods

Samples were collected according to Sohn et al. (2001)'s sequence concept. Of the six sequences defined by Sohn et al. (2001), five sandstone to conglomerate samples (PB1-1, PB1-2, PB2-1, PB2-2, and PB3) were collected from the bases of the lower five sequences (sequences 1–5) for detrital zircon analysis (Fig. 1c, Supplementary Table 1). For conglomerates, only the sandstone matrix was collected. Samples were not obtained from the uppermost sequence (sequence 6) because the outcrops are now covered by vegetation and towns.

Zircon U—Pb analysis was carried out following the processes used by Lee et al. (2021). Detrital zircon grains were extracted from the samples using conventional heavy-mineral separation methods at the Geological Department at Lund University, Sweden. The zircons were mounted in epoxy and polished. The internal structures of the zircon grains were observed by transmitted light microscopy and secondary emission, cathodoluminescence (CL), and back-scattered electron imaging, using a high-resolution field-emission–scanning electron microscope (FE–SEM; Tescan Mira 3, Brno, Czech Republic) at Lund University.

The U—Pb isotopic compositions of the zircon grains were analysed in the Laser Ablation Inductively Coupled Plasma Mass Spectrometry (LA–ICP–MS) laboratory at Lund University. The LA–ICP–MS system consists of a Teledyne Photon Machines G2 (Teledyne Technologies, Omaha, NE, USA) laser and a Bruker Aurora Elite quadrupole ICP–MS (Bruker Daltonics, Bremen, Germany). Instrument tuning was conducted with the aim of obtaining high and stable signal counts on lead isotopes, low oxide production (below 0.5 % monitoring $^{238}U/^{238}U^{16}O$ and $^{232}Th/^{232}Th^{16}O$), and Th/U ratios of 1 using NIST612 as the standard. The GJ-1 (Jackson et al., 2004) and 91,500 (Wiedenbeck et al., 1995) natural zircons were used as primary and secondary reference standards, respectively. The analytical results of the reference samples are provided in Supplementary Table 2. Each analysis was carried out with 300 shots at 10 Hz with a fluence of 2.5 J/cm^2. Baseline compositions were measured for 30 s before each measurement, and subtraction was performed with a step-forward approach. Common Pb was monitored by measuring ^{202}Hg and mass 204 ($^{204}Hg + {}^{204}Pb$). Data reduction was carried out with Iolite using the X_U_Pb_Gerchron4 DSR (Paton et al., 2010, 2011), and common-Pb correction was performed using the VizualAge DRS by Petrus and Kamber (2012). The decay constant values (λ) of ^{238}U and ^{235}U used to calculate the zircon ages were 1.55125×10^{-10}/yr and 9.8485×10^{-10}/yr, respectively (Steiger and Jäger, 1977). All uncertainties of the isotopic ratios and ages are 2σ levels. For zircon ages older and younger than 1000 Ma, $^{207}Pb/^{206}Pb$ and $^{206}Pb/^{238}U$ ages were used, respectively. The discordances (%) of the zircon ages were calculated as $[1 - (^{206}Pb/^{238}U \text{ age})/(^{207}Pb/^{235}U \text{ age})] \times 100$ and $[1 - (^{206}Pb/^{238}U \text{ age})/(^{207}Pb/^{206}Pb \text{ age})] \times 100$ for ages younger and older than 1000 Ma, respectively. The kernel density estimates (Vermeesch, 2013) were constructed using the $^{206}Pb/^{238}U$ ages and $^{207}Pb/^{206}Pb$ ages for zircon with the same criteria.

To investigate the overall provenance signals from the Doumsan fan-delta deposits, 17 samples (PH-1s, 1m, 2, 3-1, 3-2, 4–15) were collected from the middle to upper parts of the lower five sequences (sequences 1–5; Fig. 1c). In each sequence, two to four samples were obtained from

different stratigraphic positions. The depositional sequences of the Doumsan fan-delta system commonly show a crude fining-upward trend from conglomerate to siltstone; thus, the grain sizes of the collected samples vary from coarse sand to silt (Supplementary Table 1).

The samples were powdered in an agate mortar, and the powdered samples were geochemically analysed at Activation Laboratories Ltd., Ancaster, Ontario, Canada. The major-element compositions were obtained as oxides, including SiO_2, Al_2O_3, Fe_2O_3 (total Fe), TiO_2, MnO, MgO, K_2O, Na_2O, and P_2O_5 by lithium metaborate/tetraborate fusion Inductively Coupled Plasma (ICP). Detection limits for the major elements are lower than 0.01 %. The levels of the trace elements Ba, Sc, Sr, V, Y, and Zr were also measured by fusion ICP, and those of the trace elements Co, Cr, Cs, Hf, Nb, Ni, Pb, Rb, Th, and U, and the rare earth elements (La to Lu) were obtained by fusion ICP-MS. Detection limits of the trace and rare earth elements are mostly between 0.01 and 2 ppm. Detection limits of Ni and Cr are 20 ppm. Further details of the analytical procedure and data quality can be found on www.actlabs.com.

4. Results

4.1. Detrital zircon geochronology

Of the total of 659 zircon grains analysed, 561 grains provided concordant (less than ±10 % discordance) U—Pb ages, ranging from 2649 ± 19.8 Ma (Archean) to 51.6 ± 0.8 Ma (Eocene) (Supplementary Table 3). Only zircons with concordant ages are considered in the discussion below. The Th/U ratios are higher than 0.1 in all but three of the zircon grains, indicating magmatic origins (Varva et al., 1999; Hoskin and Black, 2000), as corroborated by the common observation of oscillatory zoning in CL images (Fig. 2). Most of the Cenozoic zircons are characterised by euhedral shapes; in contrast, some of the Precambrian and Mesozoic (Jurassic and Triassic) zircons tend to be more rounded than the Cenozoic grains, possibly reflecting abrasion during recycling.

Most of the zircon grains fall into three major age groups: Palaeoproterozoic (2480–1863 Ma); middle Cretaceous (124–92 Ma); and latest Cretaceous to early Eocene (79–52 Ma; Fig. 3; Table 1). Zircons of latest Cretaceous to early Eocene ages are the most common, forming 42 %–73 % of the total number. The middle Cretaceous and Palaeoproterozoic zircons represent 13 %–20 % and 4 %–22 % of the total, respectively. In addition to these three major age groups, the analysed samples contain zircons of Archean, Neoproterozoic, Palaeozoic, and Jurassic–Triassic ages. If latest Cretaceous to early Eocene zircons are excluded, the age spectra of the Doumsan fan-delta deposits are similar to those of the Cretaceous sedimentary rocks of the Hayang Group (Choi and Kwon, 2019). These Archean–Turonian-aged zircons constitute 27 % to 58 % of the total zircon population.

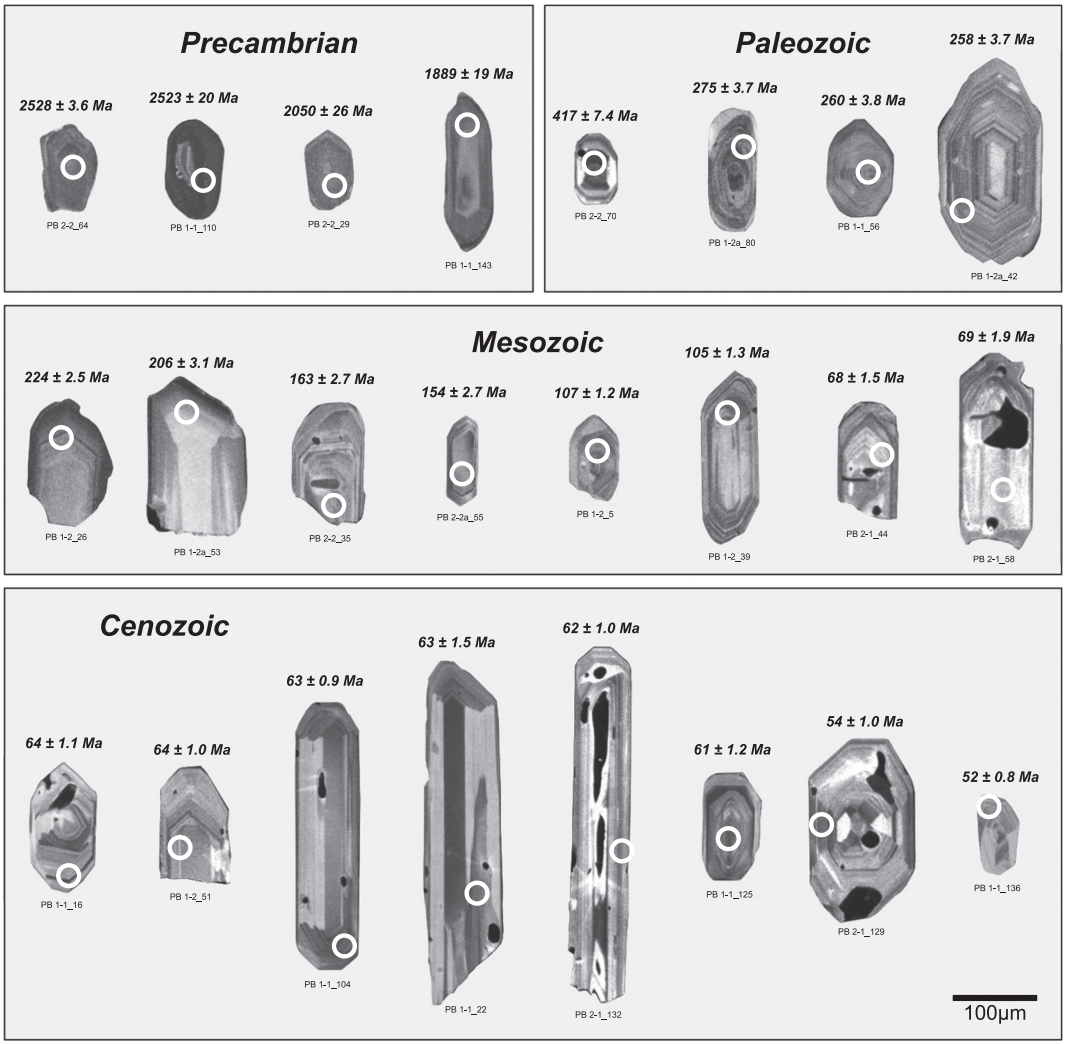

Fig. 2. Representative examples of SEM-CL images of detrital zircon grains analysed in this study. White circles are the analysis spots (diameter 25 μm). For zircons younger and older than 1000 Ma, the $^{206}Pb/^{238}U$ and $^{207}Pb/^{206}Pb$ ages are marked, respectively.

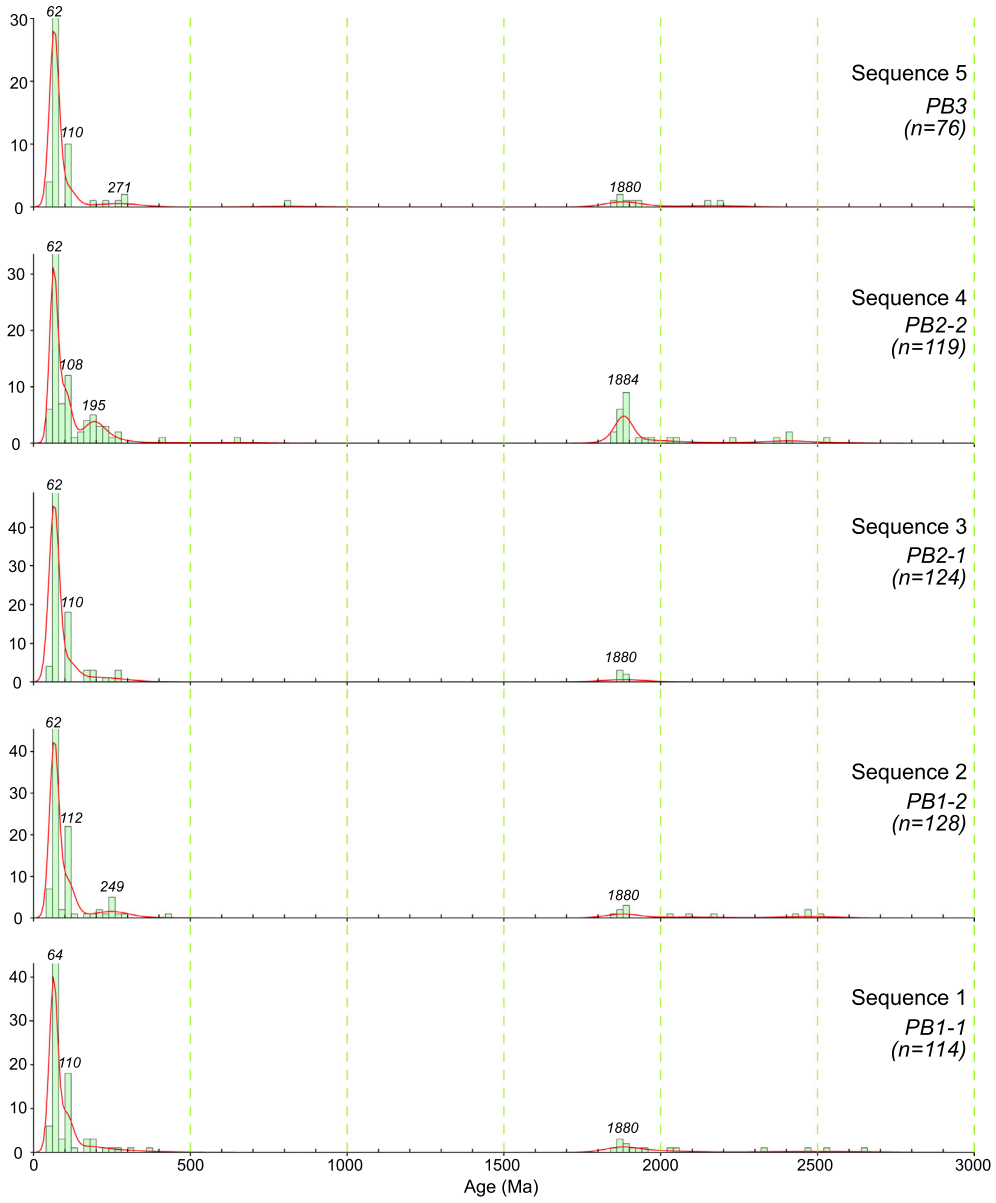

Fig. 3. Kernel density estimates and histograms of detrital zircon U—Pb ages in sequences 1–5 of the Doumsan fan-delta deposits.

All five samples yield similar age spectra, characterised by a prominent early Paleocene age peak (62–64 Ma). However, sequence 4 can be distinguished from the others by its high proportion of Palaeoproterozoic zircons (22 %), which are two to five times more abundant than the rest (4 %–11 %). Sequence 4 also contains a higher proportion of Triassic–Jurassic zircons (15 %) than the other sequences (3 %–6 %).

The latest Cretaceous to earliest Eocene zircons exhibit another major stratigraphic difference when observed in detail (Figs. 4, 5). In sequence 1, the proportion of Paleocene–Eocene zircons is 51 %, with only 7 % being of latest Cretaceous (Campanian to Maastrichtian) age. In contrast, sequence 2 contains 36 % Paleocene–Eocene zircons and 24 % latest Cretaceous zircons. The proportion of Paleocene–Eocene zircons increases again to 46 % in sequence 3, in which the percentage of latest Cretaceous zircons is 27 %, similar to that of the preceding sequence. In sequence 4, the proportion of Paleocene–Eocene zircons decreases to 34 % and that of latest Cretaceous zircons to 8 %. Lastly, sequence 5 displays age proportions similar to those of sequence 3.

4.2. Geochemical composition

Bulk-rock compositions including major, trace, and rare earth elements are presented in Supplementary Table 4.

4.2.1. Major elements

The Doumsan fan-delta deposits show a wide range of major-element compositions (Supplementary Table 4; Fig. 6), indicating wide variations in their mineralogy and/or grain size. The percentages of SiO_2 and Al_2O_3, the two most abundant major elements, are 49.9 %–72.2 % (average = 66.7 %) and 8.6 %–15.4 % (average = 13.3 %), respectively. Sequence 5 is distinguished from the rest of the sequences in exhibiting the highest SiO_2 content. Deposition of diatoms in the deep-marine environment might have added biogenic silica to sequence 5 (Um et al., 1964; Hwang et al., 1995; Sohn et al., 2001). In the major-element binary plots, sequences 3 and 4 are scattered widely, indicating their compositional heterogeneity. They are enriched in Fe_2O_3 and TiO_2 relative to sequences 1 and 2. Fe-rich minerals such as mica or clay

Table 1
Summary of the detrital zircon age distribution of the Doumsan fan-delta deposits.

Age		*PB 1-1*			*PB 1-2*			*PB 2-1*			*PB 2-2*			*PB 3*		
		Range (Ma)	n	(%)	Range (Ma)	n	(%)	Range (Ma)	n	(%)	Range (Ma)	n	(%)	Range (Ma)	n	(%)
Eocene	Ypresian (56.0–47.8 Ma)	54–52	3	2.6 %	56–54	2	1.6 %	54–53	2	1.6 %						
Paleocene	Thanetian (59.2–56.0 Ma)	58	2	1.8 %	59–56	5	3.9 %	58	1	0.8 %	59	2	1.7 %	58–57	3	3.9 %
	Selandian (61.6–59.2 Ma)	61–59	2	1.8 %	61	2	1.6 %	61–60	4	3.2 %	61–60	8	6.7 %	61–60	3	3.9 %
	Danian (66.0–61.6 Ma)	66–62	51	44.7 %	66–62	37	28.9 %	66–62	50	40.3 %	66–62	30	25.2 %	66–62	25	32.9 %
	Cenozoic total	***66–52***	***58***	***50.9 %***	***66–54***	***46***	***35.9 %***	***66–53***	***57***	***46.0 %***	***66–59***	***40***	***33.6 %***	***66–57***	***31***	***40.8 %***
Cretaceous	Maastrichtian (72.1–66.0 Ma)	70–66	7	6.1 %	72–67	29	22.7 %	71–66	33	26.6 %	71–66	10	8.4 %	71–66	20	26.3 %
	Campanian (83.6–72.1 Ma) Santonian (86.3–83.6 Ma) Coniacian (89.8–86.3 Ma)	79	1	0.9 %	76–74	2	1.6 %							74	1	1.3 %
	Turonian (93.9–89.8 Ma)				92	1	0.8 %									
	Cenomanian (100.5–93.9 Ma)	100–99	3	2.6 %	98	1	0.8 %				100–95	7	5.9 %			
	Late Cretaceous total (100.5–66.0 Ma)	***100–66***	***11***	***9.6 %***	***98–67***	***33***	***25.8 %***	***71–66***	***33***	***26.6 %***	***100–66***	***17***	***14.3 %***	***74–66***	***21***	***27.6 %***
	Albian (113–100.5 Ma)	110–101	17	14.9 %	111–101	14	10.9 %	113–102	15	12.1 %	109–101	12	10.1 %	110–101	8	10.5 %
	Aptian (125–113 Ma) Barremian (129.4–125 Ma) Hauterivian (132.9–129.4 Ma) Valanginian (139.8–132.9 Ma)	119	1	0.9 %	124–114	9	7.0 %	116–114	3	2.4 %	121	1	0.8 %	115	2	2.6 %
	Berriasian (145–139.8 Ma)	140	1	0.9 %												
	Early Cretaceous total (139.8–100.5 Ma)	***140–101***	***19***	***16.7 %***	***124–101***	***23***	***18.0 %***	***116–102***	***18***	***14.5 %***	***121–101***	***13***	***10.9 %***	***115–101***	***10***	***13.2 %***
	Cretaceous total (139.8–66.0 Ma)	***140–66***	***30***	***26.3 %***	***124–67***	***56***	***43.8 %***	***116–66***	***51***	***41.1 %***	***121–66***	***30***	***25.2 %***	***115–66***	***31***	***40.8 %***
Jurassic	Late (163.5–145.0 Ma)	163	1	0.9 %							163–153	3	2.5 %			
	Middle (174.1–163.5 Ma)	170–164	2	1.8 %							171–167	2	1.7 %			
	Early (201.3–174.1 Ma)	196–189	3	2.6 %	181–179	2	1.6 %	198–179	6	4.8 %	197–178	6	5.0 %	193	1	1.3 %
	Jurassic Total (201.3–145.0 Ma)	***196–163***	***6***	***5.3 %***	***181–179***	***2***	***1.6 %***	***198–179***	***6***	***4.8 %***	***197–153***	***11***	***9.2 %***	***193***	***1***	***1.3 %***
Triassic	Late (237–201.3 Ma)	231	1	0.9 %	224–206	3	2.3 %	224	1	0.8 %	228–203	5	4.2 %	229	1	1.3 %
	Middle (247.2–237 Ma)				242	1	0.8 %				245–237	2	1.7 %			
	Early (251.9–247.2 Ma)							251	1	0.8 %						
	Triassic Total (251.9–201.3 Ma)	***231***	***1***	***0.9 %***	***242–206***	***4***	***3.1 %***	***251–224***	***2***	***1.6 %***	***245–203***	***7***	***5.9 %***	***229***	***1***	***1.3 %***
Palaeozoic	Permian (298.9–251.9 Ma)	275–260	2	1.8 %	288–258	6	4.7 %	266–261	3	2.4 %	277–265	2	1.7 %	288–273	3	3.9 %
	Carboniferous (358.9–298.9 Ma)	311	1	0.9 %												
	Devonian (419.2–358.9 Ma)	377	1	0.9 %							417	1	0.8 %			
	Silurian (443.8–419.2 Ma) Ordovician (485.4–443.8 Ma) Cambrian (541–485.4 Ma)				421	1	0.8 %									
	Palaeozoic total (541–251.9 Ma)	***377–260***	***4***	***3.5 %***	***421–258***	***7***	***5.5 %***	***266–261***	***3***	***2.4 %***	***417–265***	***3***	***2.5 %***	***288–273***	***3***	***3.9 %***
Precambrian	Neoproterozoic (1000–541 Ma) Mesoproterozoic (1600–1000 Ma)										658	1	0.8 %	809	1	1.3 %
	Palaeoproterozoic (2500–1600 Ma)	2470–1853	13	11.4 %	2480–1856	12	9.4 %	1897–1872	5	4.0 %	2415–1843	26	21.8 %	2182–1859	8	10.5 %
	Archean (4000–2500 Ma)	2649–2523	2	1.8 %	2517	1	0.8 %				2528	1	0.8 %			
	Precambrian total (before 541 Ma)	***2649–1853***	***15***	***13.2 %***	***2517–1856***	***13***	***10.2 %***	***1897–1872***	***5***	***4.0 %***	***2528–658***	***28***	***23.5 %***	***2182–809***	***9***	***11.8 %***
Total			***114***			***128***			***124***			***119***			***76***	

minerals are enriched in sequences 3 and 4 compared with the lower two sequences. In contrast, sequences 1 and 2 have slightly higher K_2O, Na_2O, and CaO contents than the three upper sequences, indicating that the lower part of the succession contains a higher proportion of feldspar than the upper part.

4.2.2. Trace elements

Compared with upper continental crust, the Doumsan fan-delta deposits are enriched in Cs and Co, and depleted in Sr and Nb (Fig. 7). The Cs and Co enrichment is stronger in the upper three sequences (sequences 3–5) than in the lower two sequences (sequences 1–2). Ferromagnesian trace elements such as Sc, V, and Cr are also more enriched in the upper three sequences. Sr shows a strong positive relationship with CaO ($r = 0.81$), if two outliers are excluded, indicating its incorporation into Ca-feldspar. The minor proportion of carbonate minerals in the Doumsan fan-delta deposits, as indicated by the low CaO content (average = 1.6 %), may explain the Sr depletion.

4.2.3. Rare earth elements

Rare earth element (REE) compositions are presented in Fig. 8 as chondrite-normalised patterns. All the Doumsan fan-delta deposits show REE patterns characterised by enrichment of light REEs (LREEs) relative to heavy REEs (HREEs) and a negative Eu anomaly. The $(La/Yb)_n$ ratio, reflecting LREE and HREE fractionation, ranges from 5.15 to

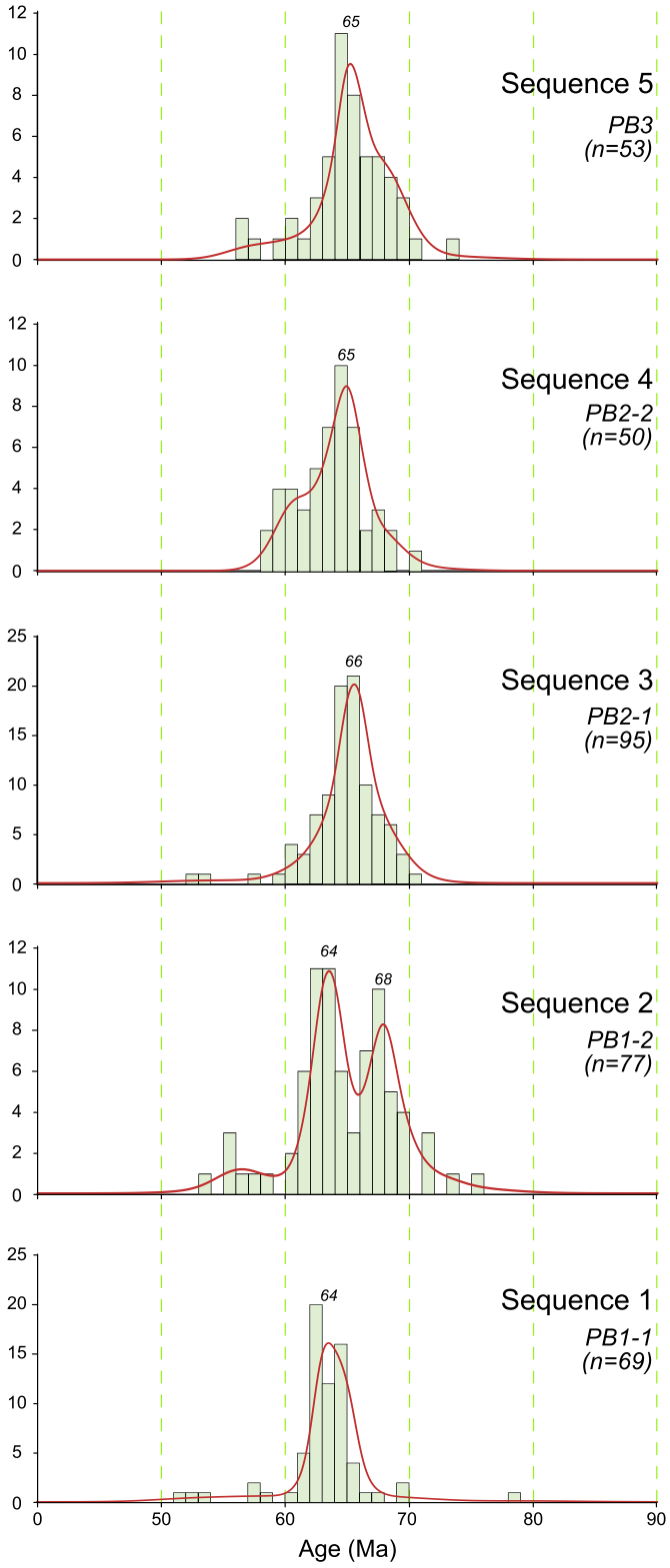

Fig. 4. Kernel density estimates and histograms of detrital zircon U–Pb ages (younger than 90 Ma) in sequences 1–5 of the Doumsan fan-delta deposits.

12.43 (average = 8.73). Most of the Doumsan fan-delta deposits exhibit $(La/Yb)_n$ ratios that are intermediate between those of Cretaceous granitic rocks (average = 10.17) and andesites (average = 7.20) of the Korean Peninsula (Lee and Kim, 2012), indicating moderate to high enrichment of LREEs relative to HREEs. The Eu/Eu^* ratios are 0.66–0.98 (average = 0.76), mostly between those of Cretaceous granitic rocks (average = 0.58) and andesites (average = 0.81) of the Korean Peninsula (Lee and Kim, 2012). Distinctive stratigraphic variations are not recognised in the $(La/Yb)_n$ and the Eu/Eu^* ratios. Compared with the Cretaceous sedimentary rocks of the Gyeongsang Basin (the Hayang Group; Lee and Lee, 2003), the Doumsan fan-delta deposits show lower $(La/Yb)_n$ ratios (average for the Hayang Group = 10.78) and higher Eu/Eu^* ratios (average for the Hayang Group = 0.64).

5. Discussion

5.1. Provenance of the Doumsan fan-delta system

Palaeocurrent data (Hwang et al., 1995; Park et al., 2013), as well as previous provenance analysis based on the clast assemblages of conglomerates (Hong et al., 1998), indicate that the sedimentary rocks of the Doumsan fan delta were derived from western source areas. In the western areas beyond the present-day basin margin, four main types of potential source rocks are exposed: (1) Cretaceous (~Cenomanian or Turonian) sedimentary rocks; (2) felsic volcanic rocks (Paleocene–earliest Eocene); (3) granitic rocks (latest Cretaceous); and (4) andesite (latest Cretaceous) (see Geological Setting for detail).

In this context, the detrital zircon age data can be used to discriminate the influence of source rocks of different ages. The high proportion of earliest Eocene to latest Cretaceous zircons in the Doumsan fan-delta deposits may reflect a strong influence of nearby igneous rocks formed during previous magmatism. The latest Cretaceous (Campanian–Maastrichtian) zircons (Table 1) could have been derived mainly from andesites or granitic rocks formed in the early stage of magmatism. In contrast, the Paleocene to earliest Eocene zircons could have come mainly from felsic volcanic rocks formed in the late stage of magmatism. The Archean to Turonian zircons would have been sourced from Cretaceous sedimentary rocks.

Geochemical data also provide information on source-rock lithology. In the La–Th–Sc ternary diagrams of Bhatia and Crook (1986), the lower two sequences plot close to the passive margin to active continental margin field, reflecting derivation from mainly felsic igneous rocks and pre-existing sedimentary rocks (Fig. 9). In contrast, some samples of the upper three sequences plot in the continental island arc field, supporting the partial derivation of sediments from more mafic rocks. However, the overall felsic composition of the Doumsan fan-delta deposits suggests that the drainage basin might not have expanded far from the boundary between granitic rocks and andesite, even at the period of maximum expansion.

A model showing the evolution of the source rock terrane was constructed using combined detrital zircon and geochemical data (Fig. 10). In the earliest stage (sequence 1), the source area might have been located close to the basin margin. A significant amount of sediment would have been derived from felsic volcanic rocks (51 %; Paleocene to Eocene zircons) and Cretaceous sedimentary rocks (42 %; Archean to Turonian zircons) adjacent to the western basin margin. The occurrence of minor Campanian to Maastrichtian zircons (7 %) suggests that some of the granitic rock might also have been included in the source area. The overall felsic composition of the sequence 1 samples (e.g., Th/Sc average = 1.36) indicates that sediment derivation from andesite was negligible or absent during this stage.

In sequence 2, the proportion of Campanian–Maastrichtian zircons rises to 24 %. The relative contribution from andesite or granitic rocks might have increased as a result of westward expansion of the source area. The felsic composition of the sequence 2 samples (e.g., Th/Sc average = 1.29) suggests that the source areas might not have expanded far west, to where andesites were exposed; thus, most of the Campanian to Maastrichtian zircons might have been derived from granitic rocks.

The zircon age proportions of sequence 3 are similar to those of sequence 2, except for a decrease in Archean–Turonian zircons (27 %), probably representing decrease of sediment input from the

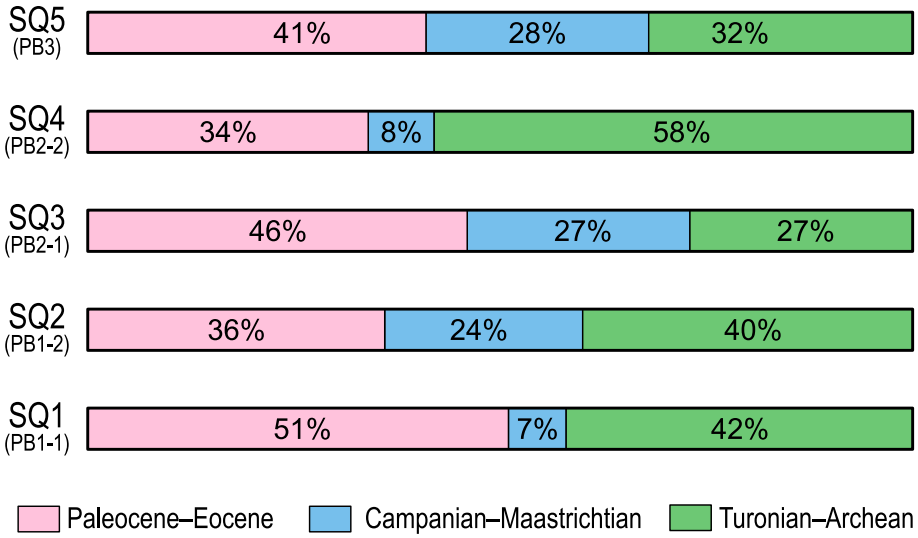

Fig. 5. Relative proportions of Archean–Turonian, Campanian–Maastrichtian, and Paleocene–Eocene zircons in sequences 1–5 of the Doumsan fan-delta deposits. Note the marked increases of the Campanian to Maastrichtian age proportion from sequences 1 to 2 and 4 to 5, and of the Turonian to Archean age proportion from sequences 3 to 4.

Cretaceous sedimentary rocks. The sequence 3 samples display the lowest Zr and Hf levels with the lowest Zr/Sc ratio (average = 18.91), supporting decreased sediment input from the Cretaceous sedimentary rocks during deposition of this sequence. The source areas might have expanded further to the west where andesites were exposed, resulting in less felsic chemical composition of the sequence 3 (e.g., Th/Sc average = 0.92).

The proportion of Archean–Turonian zircons is highest in sequence 4 (58 %), suggesting a notable increase in the sediment contribution from Cretaceous sedimentary rocks. The highest Zr (average = 218 ppm) and Hf (average = 5.4 ppm) levels with increased Zr/Sc ratio (average = 26.86) are also consistent with recycling of pre-existing sedimentary rocks (McLennan et al., 1993). The source area might have become restricted to the area

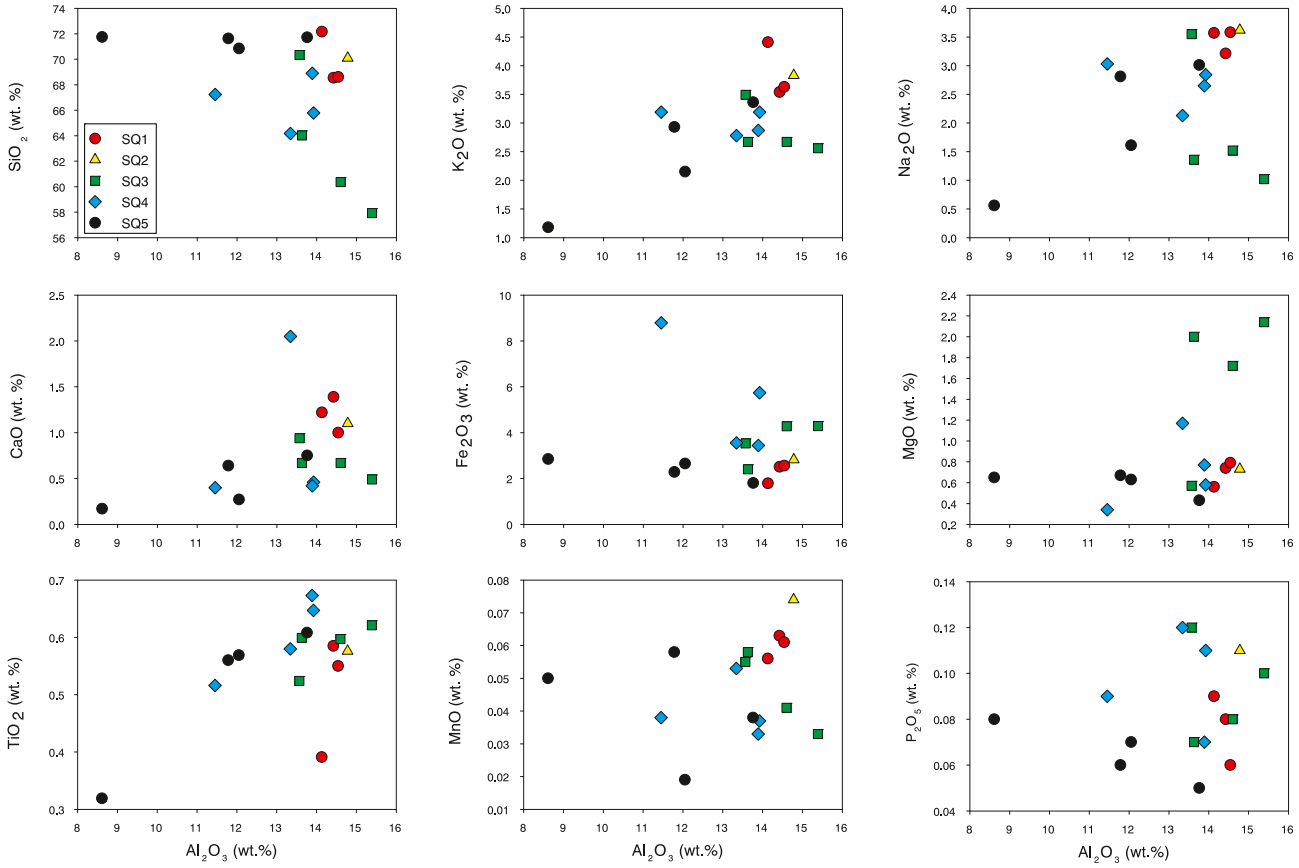

Fig. 6. Major-element binary plots of the Doumsan fan-delta deposits. An outlier (PH15) showing anomalously high CaO (14.7 %) and LOI (12.5 %) is excluded from the plots.

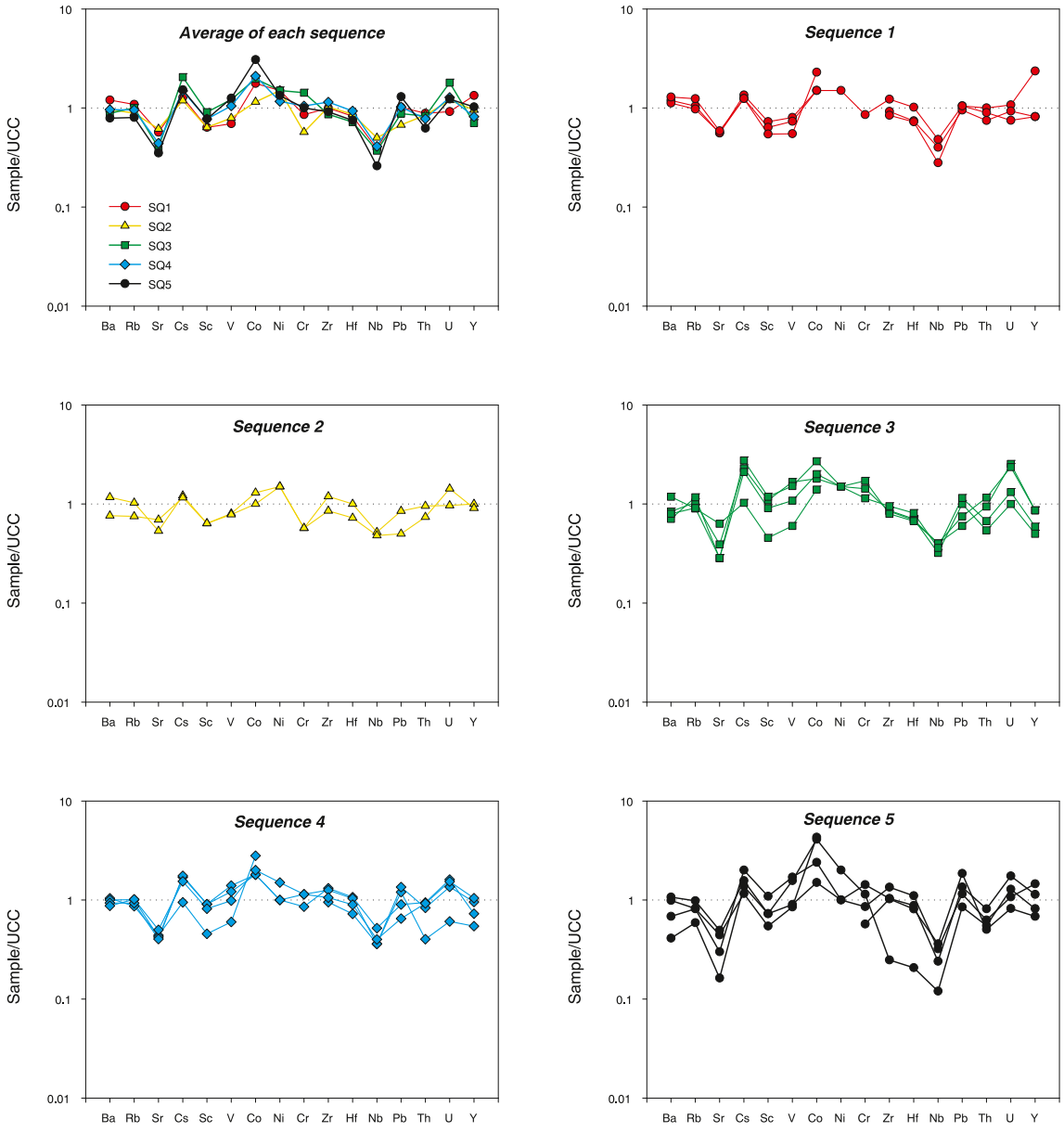

Fig. 7. Trace-element compositions of the Doumsan fan-delta deposits normalised against upper continental crust (Taylor and McLennan, 1985).

adjacent to the basin margin, where Cretaceous sedimentary rocks were dominantly exposed. In addition, meter-long intrabasinal sandstone and mudstone clasts reported from sequence 4 (Sohn et al., 2001, fig. 9) indicate that at least part of the lower sequences might have been reworked and incorporated into sequence 4. Nonetheless, the influence of sediment input from the lower sequences does not appear to have been significant, as indicated by the distinct detrital zircon population and geochemical composition of sequence 4 in comparison to those of the lower sequences.

Sequence 5 exhibits zircon age distributions that are highly similar to those of sequence 3. The geochemical composition is also similar to that of sequence 3, with a less felsic composition (e.g., Th/Sc = 0.80). The source areas might have expanded again westward over the granitic rock terrane, to include andesite.

5.2. Fan and drainage basin size

A fan and its drainage basin may have a positive relationship in terms of plan-view size, following the equation $A_f = cA_d^n$, where A_f = fan size, A_d = drainage basin size, and c and n are empirical constants (e.g., Harvey, 1989; Allen and Hovius, 1998; Blair and McPherson, 2009). The relationship can be highly variable because the two empirical constants (c and n) are controlled by the mixed influence of tectonics, climatic conditions, and bedrock lithology (Bull, 1977; Harvey, 1989; Lecce, 1991; Blair, 1999; Mather et al., 2000). The Doumsan fan-delta system formed mainly as a Gilbert-type fan-delta under the influence of major downfaulting in the early stage. A large volume of accommodation space was generated by the abrupt tectonic subsidence, along with a rapid rise in relative sea-level. In an area where tectonic subsidence is dominant, a large accommodation space can allow vertical accumulation of sediments in a fan, resulting in generation of a small fan in terms of plan-view size (Allen and Densmore, 2000). Whipple and Trayler (1996) and Calvache et al. (1997) showed that the size of a fan and its drainage basin can be similar when tectonic subsidence is small, whereas the fan can be much smaller than the drainage basin when tectonic subsidence is large.

The Doumsan fan-delta system was initially ~3 km in radius (sequence 1) and subsequently expanded to ~6 km (sequence 5),

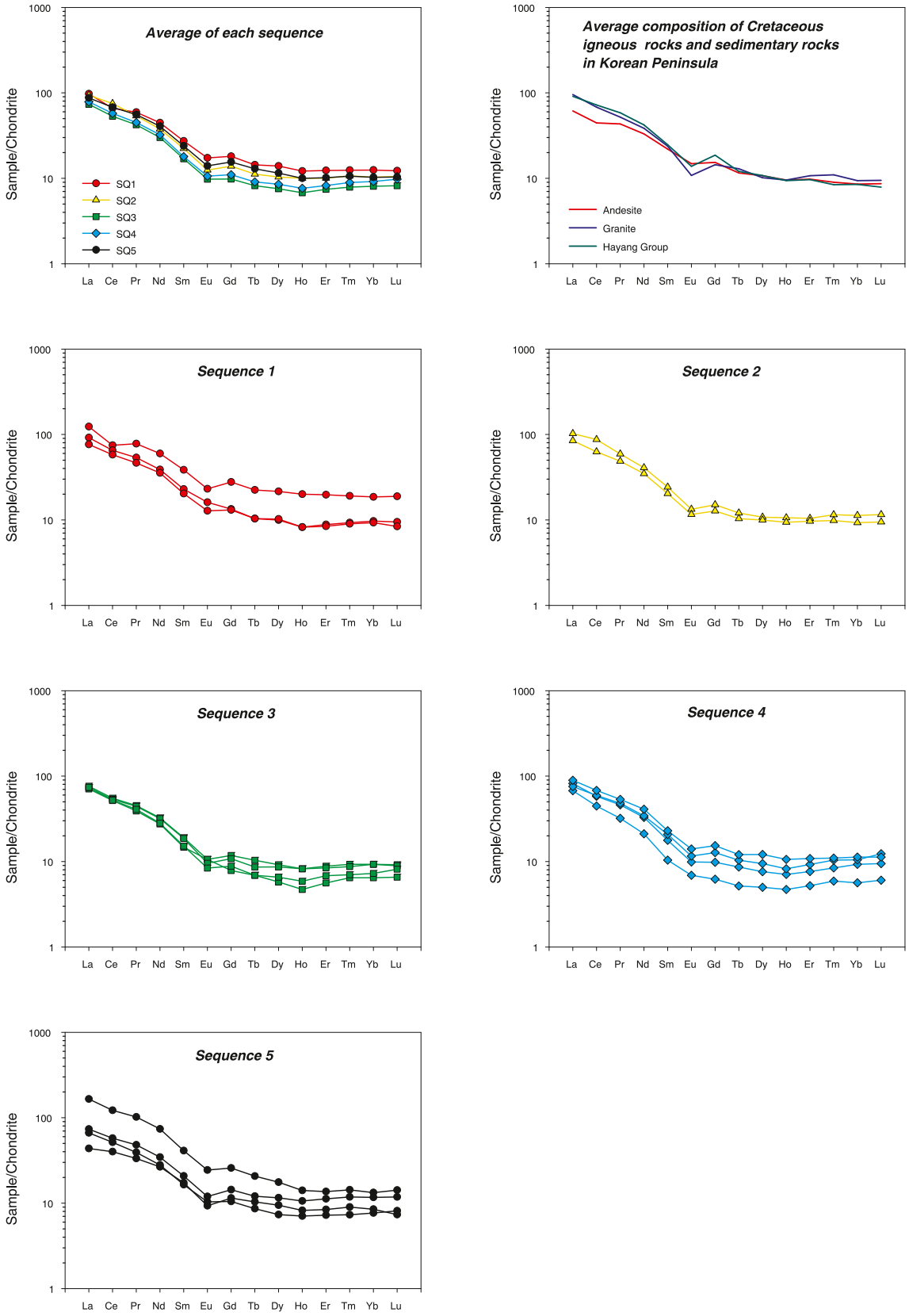

Fig. 8. Chondrite-normalised REE patterns of the Doumsan fan-delta deposits. The chondrite normalising factors are adopted from Taylor and McLennan (1985). Average REE compositions of some Cretaceous igneous rocks and Cretaceous sedimentary rocks (the Hayang Group) are also presented for comparison (Lee and Lee, 2003; Lee and Kim, 2012).

according to previous sedimentological studies (Hwang et al., 1995; Sohn et al., 2001). In terms of plan-view size, the fan might have occupied ~9 km^2 in the initial stage and a maximum of ~38 km^2 later. Our provenance data suggest that the drainage basin initially extended 2–4 km from the basin margin and mostly contained the adjacent felsic volcanic rocks and Cretaceous sedimentary rocks. In the later stage

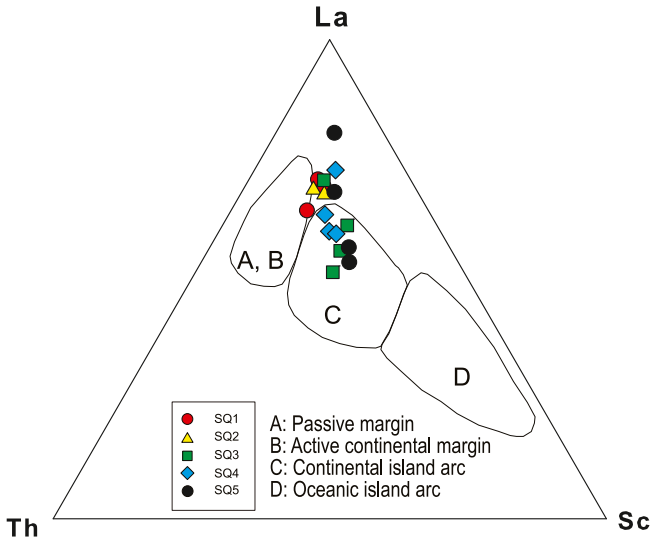

Fig. 9. La–Th–Sc ternary diagram (Bhatia and Crook, 1986) of the Doumsan fan-delta deposits.

(sequences 3 and 5), the drainage basin might have extended >10 km from the basin margin to the andesite terrene.

According to Hovius (1996), drainage basins developed along linear mountain belts may show a narrow aspect ratio (length/width) range of 1.91–2.23, with an average value of 2.1. Talling et al. (1997) reported that the drainage basins developed on fault blocks have an average aspect ratio of 2.5, although their aspect ratios are more variable than those of linear mountain belts, ranging from 1.41 to 4.06. If an aspect ratio of 2.5 is adopted, the drainage basin of the Doumsan fan-delta might have measured 2–6 km^2 in the earliest stage and later expanded to >40 km^2. According to Blair and McPherson (2009), fan size may range from 1.6 to 155.3 km^2 when the drainage basin is 50 km^2 in size, but a compilation of published data has shown that most values are between 5 and 60 km^2 (Blair and McPherson, 2009, fig. 14.23). These calculations suggest that our provenance analysis is reasonable.

Comparison of the sizes of the fan and the drainage basin is also instructive. The Doumsan fan delta possesses a relatively large fan size (up to 38 km^2) relative to the drainage area (>40 km^2). Considering that subsidence was active during formation of the fan delta, the drainage area is relatively small. Thus, the relatively large fan size compared with the drainage basin might not have been controlled dominantly by tectonism (Sohn et al., 2001). During the development of the Doumsan fan-delta systems (during the middle Miocene), the global climate was much warmer than that of the present day as a result of elevated atmospheric CO_2 (Zachos et al., 2001; You et al., 2009; Foster et al., 2012). In East Asian regions including the South China Sea, Korean Peninsula, and Japan, the precipitation rate would probably have increased as a result of intensification of the summer monsoon, resulting in moderate to intense chemical weathering in source areas (Wei et al., 2006; Wan et al., 2009; Hatano et al., 2019). Increased precipitation in the source area might have increased the rate of erosion (Oguchi and Ohmori, 1994) and sediment transport efficiency to the fan (Milana and Ruzycki, 1999), increasing the relative size of the fan.

5.3. Drainage basin evolution and tectonic implications (eustasy vs tectonism)

Planktonic foraminifera faunas indicate that most of the Pohang Basin fills were deposited between ca. 17 and 10.5 Ma (Kim, 1990; Yi and Yun, 1995). Major crustal extension and subsidence occurred at ca. 17 Ma in the Pohang Basin and nearby areas, from the southeast Korean Peninsula to the southwestern margin of Japan, resulting in an abrupt transition from shallow- to deep-marine environments (Ingle, 1992; Byun, 1995; Kim, 1999) and development of a Gilbert-type fan-delta system in the Pohang Basin (sequence 2). Previous sedimentological studies have suggested that tectonism diminished following rapid basin subsidence at 17 Ma, and that the development of erosional boundaries and sedimentary sequences (sequences 3–6) were mainly controlled by third-order glacioeustatic sea-level changes (Haq et al., 1987) between 17 and 10.5 Ma (Sohn et al., 2001). The universal application of the Haq curve for sequence stratigraphic interpretation, however, has been questioned (Miall, 1992; Miall and Miall, 2001, 2002), on the basis that the Haq curve was not based on accurate and precise chronostratigraphic data (Miall, 1992) and that regional tectonic activities can commonly be overprinted by eustatic sea-level changes (Plyusnina et al., 2016; Ruban, 2016). In tectonically active regions, local tectonic events often control sediment supply and accommodation, resulting in sequential development of sedimentary successions (Coakley and Watts, 1991; Posamentier and Allen, 1993; Dorsey and Umhoefer, 2000). This appears to apply to the Pohang Basin.

Provenance data in this study indicate abrupt shrinkage of the drainage basin during deposition of sequence 4, implying that there was another tectonic pulse after 17 Ma. Based on biostratigraphic studies, sequence 4 formed at ca. 15 Ma, when the Korea Strait, between the southeast Korean Peninsula and southwestern Japan, was closed and inflow of the Kuroshio Warm Current into the East Sea was blocked (Jung, 1993; Byun, 1995; Kim, 1999). This interval coincides with extensive folding of the Korea Strait under a compressional stress regime caused by the collision of the Philippine Plate and Japan (Kim et al., 2008; Son et al., 2013, 2015). However, it is also possible that a eustatic sea-level fall at ca. 15.5 Ma (Haq et al., 1987) could be correlated with the base of sequence 4 (Sohn et al., 2001).

We suggest that crustal uplift at ca. 15 Ma in the southeast Korean Peninsula, including the Pohang Basin, might have caused shrinkage of the drainage basin during deposition of sequence 4 by re-activation of the border faults and uplift of the adjacent source area (Fig. 11) (e.g., Olivarius et al., 2014; Figueiredo et al., 2016). The occurrence of intrabasinal mega-clasts in sequence 4 (Sohn et al., 2001, fig. 9) supports tectonic uplift of both the underlying sequences and source areas (Whittaker et al., 2009; Allen and Heller, 2012). This 15-Ma tectonic event was not previously recognised in the fan delta systems of the Pohang Basin (e.g., Hwang et al., 1995; Hong et al., 1998; Sohn et al., 2001; Sohn and Son, 2004), although an abrupt compositional change of basaltic magma from subalkaline to alkaline and the cessation of the clockwise block rotation inferred from palaeomagnetic studies suggest that this tectonic event also influenced the Pohang Basin (Moon et al., 2000; Choi et al., 2013; Son et al., 2013, 2015). Our study demonstrates that detailed provenance studies can be helpful in recognising subtle and previously undetected regional tectonic influences on sedimentary systems. Further studies of precise geochronological analysis for the Doumsan fan-delta systems are required to discriminate between tectonic and eustatic influences.

6. Conclusions

Combined detrital zircon and geochemical data from the Miocene Doumsan fan delta, Pohang Basin, SE Korea, demonstrate a million-year-scale provenance change controlled by eustasy and tectonics. The provenance study shows that the lower five sequences of the Doumsan fan delta experienced gradual expansion (sequences 1–3), followed by abrupt shrinkage (sequence 4) and subsequent re-expansion of the drainage basin from ca. 17 to 10.5 Ma. This sequence development has previously suggested to have been controlled by eustatic sea-level changes. Our results instead suggest that a regional collisional tectonic event at ca. 15 Ma induced uplift of the source area, resulting in shrinkage of the drainage basin. The relatively large fan sizes compared with the drainage basin area inferred in this study can be attributed to the warm, humid climate of East Asia during the middle Miocene. This study demonstrates that it is possible to distinguish approximately

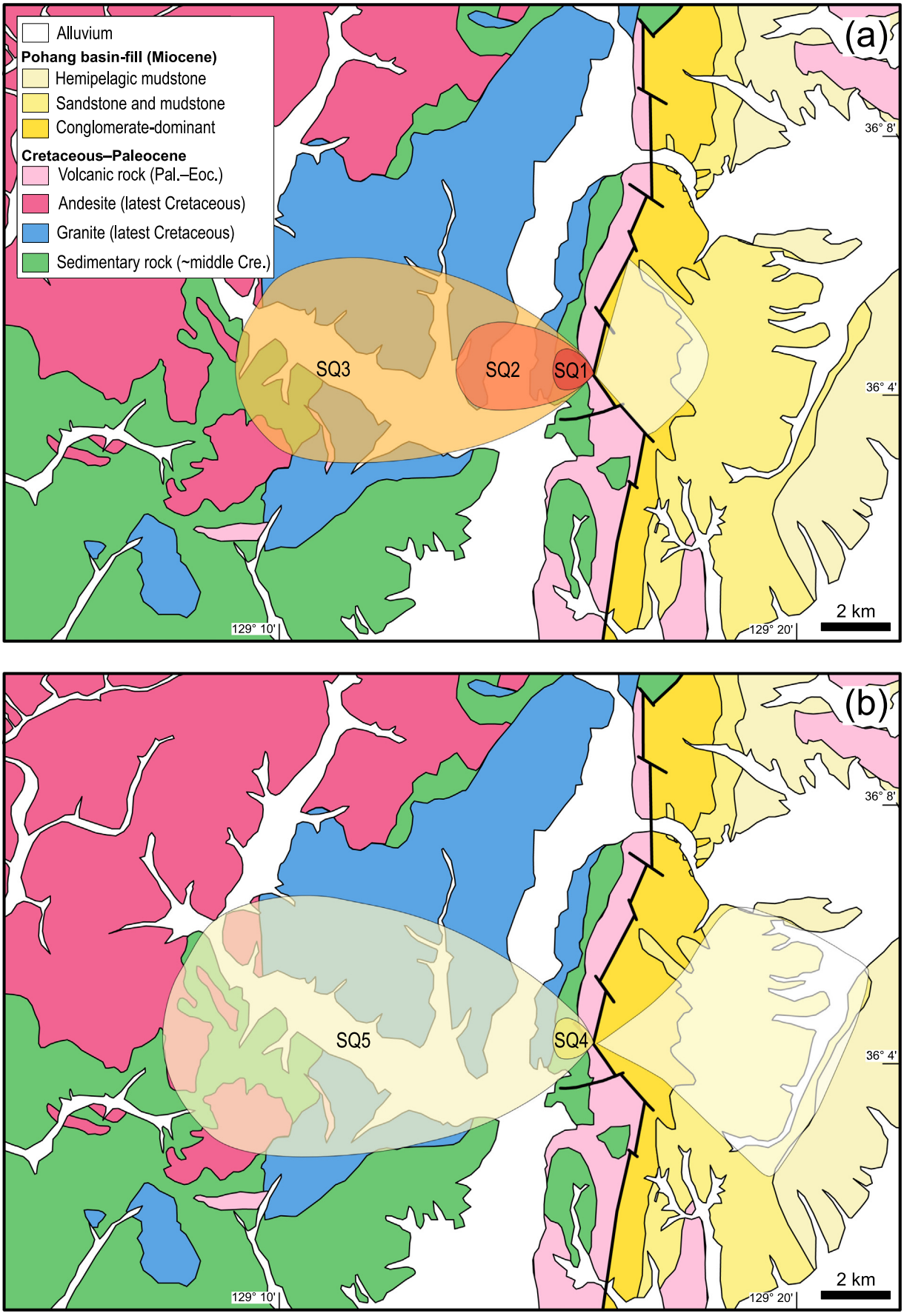

Fig. 10. Estimated areas of the drainage and fan of the Doumsan fan-delta sequences. (a) Initial stage of the drainage and fan areas (sequences 1–3). (b) Later stage of the drainage and fan areas (sequences 4 and 5). Abbreviations: Cre., Cretaceous; Eoc., Eocene; Pal., Paleocene.

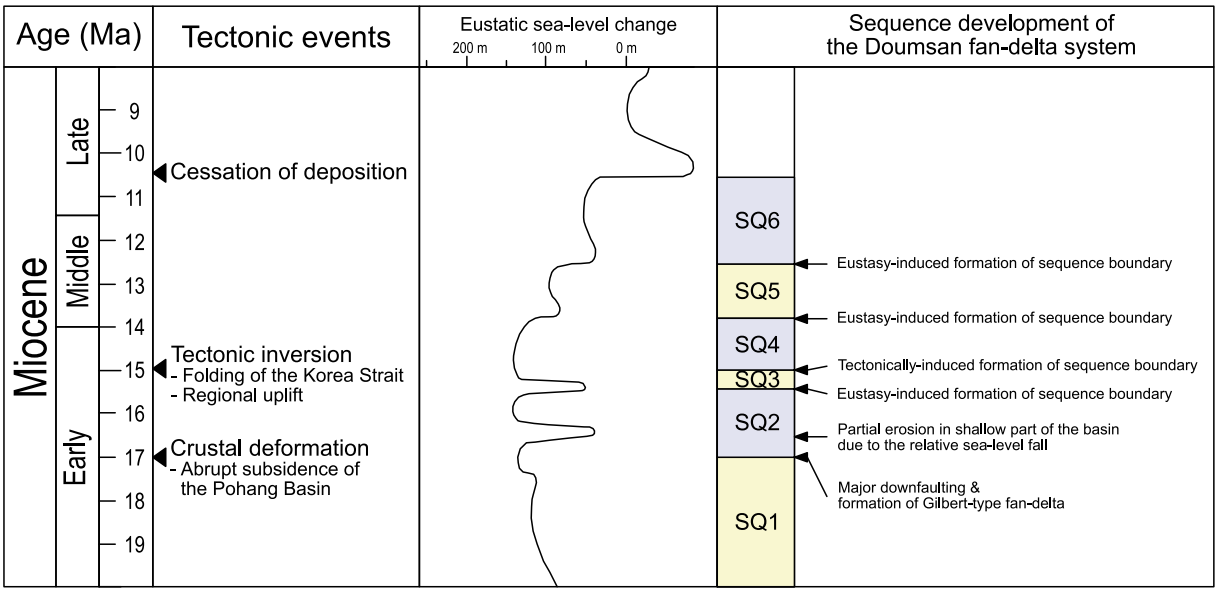

Fig. 11. Sequence development model of the Doumsan fan-delta deposits (modified after Sohn et al., 2001, fig. 14), reflecting regional tectonic events (Son et al., 2015) and eustatic sea-level changes (Haq et al., 1987). The sequence boundaries below sequences 2 and 4 might have formed under the influence of regional tectonism at around 17 and 15 Ma, respectively. The rest of the sequence boundaries might reflect eustatic sea-level falls.

contemporaneous but distinctly different influences in the successive development of fan deltas and their drainage basins from the geologic record, which may help to understand the controlling factors of fan-delta systems on long timescales.

Supplementary data to this article can be found online at https://doi.org/10.1016/j.sedgeo.2022.106180.

Declaration of competing interest

The authors declare the following financial interests/personal relationships which may be considered as potential competing interests: Jeong-Hyun Lee reports financial support was provided by National Research Foundation of Korea. Taejin Choi reports financial support was provided by National Research Foundation of Korea. Sung Hi Choi reports financial support was provided by National Research Foundation of Korea. Hyojong Lee reports financial support was provided by Korea Institute of Geoscience and Mineral Resources.

Acknowledgements

We are very grateful to Andrew Miall and an anonymous reviewer for helpful comments and suggestions that improved the final manuscript, and to Catherine Chagué for expert editorial guidance. This study was supported by the Basic Research Project of the Korea Institute of Geoscience and Mineral Resources to HL (GP2020-006), and by National Research Foundation of Korea grants to JHL (2022R1A2B5B02001184), to TC (2020R111A3072160), and to SHC (2021R1A4A5026233).

References

Allen, P.A., 2008. From landscapes into geological history. Nature 451, 274–276.
Allen, P.A., Densmore, A.L., 2000. Sediment flux from an uplifting fault block. Basin Research 12, 367–380.
Allen, P.A., Heller, P.L., 2012. Dispersal and preservation of tectonically generated alluvial gravels in sedimentary basins. In: Cathy, B., Antonio, A. (Eds.), Tectonics of Sedimentary Basins: Recent Advances. Blackwell Publishing Ltd., pp. 111–130.
Allen, P.A., Hovius, N., 1998. Sediment supply from landslide-dominated catchments: implications for basin-margin fans. Basin Research 10, 19–35.
Bhatia, M.R., Crook, K.A.W., 1986. Trace element characteristics of graywackes and tectonic setting discrimination of sedimentary basins. Contributions to Mineralogy and Petrology 92, 181–193.
Blair, T.C., 1999. Cause of dominance by sheetflood vs. debris-flow processes on two adjoining alluvial fans, Death Valley, California. Sedimentology 46, 1015–1028.
Blair, T.C., McPherson, J.G., 2009. Processes and forms of alluvial fans. In: Parsons, A.J., Abrahams, A.D. (Eds.), Geomorphology of Desert Environments, 2nd ed. Springer, pp. 413–467.
Bull, W.B., 1977. The alluvial-fan environment. Progress in Physical Geography 1, 222–270.
Byun, H., 1995. Cenozoic dinoflagellate cysts from the Pohang Basin and the southern margin of the Ulleung Basin. (Ph.D. Thesis).Chungnam National University, Daejeon 283 pp (in Korean with English abstract).
Calvache, M.L., Viseras, C., Fernandez, J., 1997. Controls on fan development - evidence from fan morphometry and sedimentology; Sierra Nevada, SE Spain. Geomorphology 21, 69–84.
Cheon, Y., Son, M., Song, C.W., Kim, J.-S., Sohn, Y.K., 2012. Geometry and kinematics of the Ocheon Fault system along the boundary between the Miocene Pohang and Janggi basins, SE Korea, and its tectonic implications. Geosciences Journal 16, 253–273.
Cheong, C.-S., Kim, N., 2012. Review of radiometric ages for Phanerozoic granitoids in southern Korean Peninsula. Journal of the Petrological Society of Korea 21, 173–192 (in Korean with English abstract).
Choi, T., Kwon, M.G., 2019. Depositional age and provenance of the sandstones in the Cretaceous Euiseong subbasin inferred by detrital zircon U-Pb age dating. Journal of the Geological Society of Korea 55, 551–581 (in Korean with English abstract).
Choi, H.-O., Choi, S.H., Lee, D.-C., Kang, H.-C., 2013. Geochemical evolution of basaltic volcanism within the Tertiary basins of southeastern Korea and the opening of the East Sea (Sea of Japan). Journal of Volcanology and Geothermal Research 249, 109–122.
Chough, S.K., Hwang, I.G., Choe, M.Y., 1990. The Miocene Doumsan fan-delta, Southeast Korea: a composite fan-delta system in back-arc margin. Journal of Sedimentary Research 60, 445–455.
Coakley, B.J., Watts, A.B., 1991. Tectonic controls on the development of unconformities: the North Slope, Alaska. Tectonics 10, 101–130.
Crosta, G.B., Frattini, P., 2004. Controls on modern alluvial fan processes in the central Alps, northern Italy. Earth Surface Processes and Landforms 29, 267–293.
Densmore, A.L., Allen, P.A., Simpson, G., 2007. Development and response of a coupled catchment fan system under changing tectonic and climatic forcing. Journal of Geophysical Research 112, F01002.
Dorsey, R.J., Umhoefer, P.J., 2000. Tectonic and eustatic controls on sequence stratigraphy of the Pliocene Loreto basin, Baja California Sur, Mexico. Geological Society of America Bulletin 112, 177–199.
Fabbri, O., Charvet, J., Fournier, M., 1996. Alternate senses of displacement along the Tsushima fault system during the Neogene based on fracture analyses near the western margin of the Japan Sea. Tectonophysics 257, 275–295.
Figueiredo, F.T., Almeida, R.P., Freitas, B.T., Marconato, A., Carrera, S.C., Turra, B.B., 2016. Tectonic activation, source area stratigraphy and provenance changes in a rift basin: the Early Cretaceous Tucano Basin (NE-Brazil). Basin Research 28, 433–445.
Foster, G.L., Lear, C.H., Rae, J.W.B., 2012. The evolution of pCO_2, ice volume and climate during the middle Miocene. Earth and Planetary Science Letters 341-344, 243–254.
Han, J.H., Kwak, Y.H., Son, J.D., Son, B.K., 1987. Tectonic Evolution and Depositional Environments of the Tertiary Sedimentary Basin, Southeastern Part of Korea (II) Korea Institute of Energy and Resources KR-86-2-(B), 109 pp (in Korean).

Haq, B.U., Hardenbol, J., Vail, P.R., 1987. Chronology of fluctuating sea levels since the Triassic. Science 235, 1156–1167.
Harvey, A.M., 1989. The occurrence and role of arid zone alluvial fans. In: Thomas, D.S.G. (Ed.), Arid Zone Geomorphology: Process, Form and Change in Dry Lands. John Wiley & Sons, Ltd., London, pp. 136–158.
Harvey, A.M., Silva, P.G., Mather, A.E., Goy, J.L., Stokes, M., Zazo, C., 1999. The impact of Quaternary sea-level and climatic change on coastal alluvial fans in the Cabo de Gata ranges, southeast Spain. Geomorphology 28, 1–22.
Hatano, N., Yoshida, K., Sasao, E., 2019. Effects of grain size on the chemical weathering index: a case study of Neogene fluvial sediments in southwest Japan. Sedimentary Geology 386, 1–8.
Hong, S.W., Chough, S.K., Hwang, I.G., 1998. Provenance of coarse-grained detritus in fan-delta systems, Miocene Pohang Basin, SE Korea: implications for boundary fault movements. Geosciences Journal 2, 46–58.
Hoskin, P.W.O., Black, L.P., 2000. Metamorphic zircon formation by solid-state recrystalization of protolith igneous zircon. Journal of Metamorphic Geology 18, 423–439.
Hovius, N., 1996. Regular spacing of drainage outlets from linear mountain belts. Basin Research 8, 29–44.
Hwang, I.G., 1993. Fan-Delta Systems in the Pohang Basin (Miocene), SE Korea. (Ph.D. Thesis).Seoul National University 923 pp.
Hwang, S.K., 2002. Collapse type and evolution of the Guamsan Caldera, southeastern Cheongsong, Korea. Journal of the Geological Society of Korea 38, 199–216 (in Korean with English abstract).
Hwang, S.K., 2017. SHRIMP U-PB dating and volcanic processes of the volcanic rocks in the Guamsan Caldera, Cheongsong, Korea. Economic and Environmental Geology 50, 467–476 (in Korean with English abstract).
Hwang, I.G., Chough, S.K., 1990. The Miocene Chunbuk Formation, southeastern Korea: marine Gilbert-type fan-delta system. In: Colella, A., Prior, D.B. (Eds.), Coarse-grained Deltas. International Association of Sedimentologists Special Publication, pp. 235–254.
Hwang, I.G., Chough, S.K., Hong, S.W., Choe, M.Y., 1995. Controls and evolution of fan delta systems in the Miocene Pohang Basin, SE Korea. Sedimentary Geology 98, 147–179.
Hwang, S.K., Jo, I.H., Yi, K., 2016. SHRIMP zircon U-Pb dating and stratigraphic relationship of the Bunam stock and Muposan tuff, Cheongsong. Journal of the Geological Society of Korea 52, 405–419 (in Korean with English abstract).
Hwang, S.K., Jo, I.H., Yi, K., 2017. SHRIMP U-Pb datings and igneous processes of the igneous rocks around the Myeonbongsan caldera, Cheongsong, Korea. Journal of the Geological Society of Korea 53, 781–796 (in Korean with English abstract).
Hwang, S.K., Jo, I.H., Son, Y.S., Song, K.-Y., Yi, K., 2019a. SHRIMP U-Pb zircon dating and volcanic process of the volcanic rocks around the Jayang Caldera, northern Yeongcheon, Korea. Journal of the Petrological Society of Korea 28, 237–249 (in Korean with English abstract).
Hwang, S.K., Kim, S.W., Kim, S.-K., Ahn, U.S., Jo, I.H., Lee, S.J., Kim, J.J., 2019b. Chronostratigraphic implication of the Yucheon Group in Gyeongsang basin, Korea. Journal of the Geological Society of Korea 55, 633–647 (in Korean with English abstract).
Hwang, I.G., Son, J., Cho, S., 2021. Event stratigraphy of Yeonil Group, Pohang Basin: based on correlation of 21 deep cores and outcrop sections. Journal of the Geological Society of Korea 57, 647–678 (in Korean with English abstract).
Ingle, J.J.C., 1992. Subsidence of the Japan Sea: stratigraphic evidence from ODP sites and onshore sections. Proceedings of the Ocean Drilling Program, Scientific Reports 127 (128), 1197–1218.
Itoh, Y., 2001. A Miocene pull-apart deformation zone at the western margin of the Japan Sea back-arc basin: implications for the back-arc opening mode. Tectonophysics 334, 235–244.
Jackson, S.E., Pearson, N.J., Griffin, W.L., Belousova, E.A., 2004. The application of laser ablation-inductively coupled plasma-mass spectrometry to in situ U–Pb zircon geochronology. Chemical Geology 211, 47–69.
Jin, M.-S., Kim, S.-J., Shin, S.-C., 1988. K/Ar and fission-track dating for volcanic rocks in the P'ohang-Kamp'o area. Korea Institute of Energy and Resources, Research Report KD-87-27, 51–88 (in Korean).
Jin, M.-S., Kim, S.-J., Shin, S.-C., Lee, J.-Y., 1989. K/Ar and fission-track datings for granites and volcanic rocks in the southeastern part of the Korean Peninsula, Research on Isotopic Geology. Korea Institute of Energy and Resources, Research Report KD-88-6D, 53–84 (in Korean).
Jolivet, L., Tamaki, K., 1992. Neogene kinematics in the Japan Sea region and volcanic activity of the Northeast Japan Arc. Proceedings of the Ocean Drilling Program, Scientific Reports 127-128, 1311–1331.
Jung, K.K., 1993. Benthic foraminiferal assemblages and paleoenvironmental analysis of the Miocene in the Pohang Basin, Korea. Journal of the Geological Society of Korea 29, 464–476.
Kim, W.H., 1990. Significance of early to middle Eocene planktonic foraminiferal biostratigraphy of the E-core in the Pohang Basin, Korea. Journal of the Paleontological Society of Korea 6, 144–164 (in Korean with English abstract).
Kim, I.-S., 1992. Origin and tectonic evolution of the East Sea (Sea of Japan) and the Yangsan fault system: a new synthetic interpretation. Journal of the Geological Society of Korea 28, 84–109 (in Korean with English abstract).
Kim, J.-M., 1999. Early Neogene biochemostratigraphy of Pohang Basin: a paleoceanographic response to the early opening of the Sea of Japan (East Sea). Marine Micropaleontology 36, 269–290.
Kim, H., Song, C.W., Kim, J.-S., Son, M., Kim, I.-S., 2008. Tertiary geological structures and deformation history of the southern Tsushima Island, Japan. Journal of the Geological Society of Korea 44, 175–798 (in Korean with English abstract).
Kim, S.W., Kwon, S., Park, S.-I., Lee, C., Cho, D.-L., Lee, H.-J., Ko, K., Kim, S.J., 2016. SHRIMP U–Pb dating and geochemistry of the Cretaceous plutonic rocks in the Korean Peninsula: A new tectonic model of the Cretaceous Korean Peninsula. Lithos 262, 88–106.
Lecce, S.A., 1991. Influence of lithologic erodibility on alluvial fan area, western White Mountains, California and Nevada. Earth Surface Processes and Landforms 16, 11–18.
Lee, S.-G., Kim, D.Y., 2012. Geochemical composition of the continental crust in Korean Peninsula. Journal of the Petrological Society of Korea 21, 113–128.
Lee, J.I., Lee, Y.I., 2003. Geochemistry and provenance of Lower Cretaceous Sindong and Hayang mudrocks, Gyeongsang Basin, southeastern Korea. Geosciences Journal 7, 107–122.
Lee, T.-H., Yi, K., Cheong, C.-S., Jeong, Y.-J., Kim, N., Kim, M.-J., 2014. SHRIMP U-Pb Zircon Geochronology and Geochemistry of Drill Cores from the Pohang Basin. The Journal of the Petrological Society of Korea 23, 167–185 (in Korean with English abstract).
Lee, T.H., Park, K.H., Yi, K., 2018. SHRIMP U–Pb ages of detrital zircons from the Early Cretaceous Nakdong Formation, South East Korea: Timing of initiation of the Gyeongsang Basin and its provenance. Island Arc 27, e12258.
Lee, J.-H., Oh, M.-K., Choi, T., 2021. Recognition of the "Great Unconformity" in the eastern Sino-Korean Block: Insights from the Taebaek Group, Korea. Precambrian Research 364, 106363.
Mather, A.E., Harvey, A.M., Stokes, M., 2000. Quantifying long-term catchment changes of alluvial fan systems. Geological Society of America Bulletin 112, 1825–1833.
McLennan, S.M., Hemming, S., McDaniel, D.K., Hanson, G.N., 1993. Geochemical approaches to sedimentation, provenance, and tectonics. Geological Society of America Special Papers 284, 21–40.
Miall, A.D., 1992. The Exxon global cycle chart: an event for every occasion? Geology 20, 787–790.
Miall, A.D., Miall, C.E., 2001. Sequence stratigraphy as a scientific enterprise: the evolution and persistence of conflicting paradigms. Earth Science Reviews 54, 321–348.
Miall, C.E., Miall, A.D., 2002. The Exxon factor: the roles of academic and corporate science in the emergence and legitimation of a new global model of sequence stratigraphy. Sociological Quarterly 43, 307–334.
Milana, J.P., Ruzycki, L., 1999. Alluvial-fan slope as a fuction of sediment transport efficiency. Journal of Sedimentary Research 69, 553–562.
Moon, T.-H., Son, M., Chang, T.-W., Kim, I.-S., 2000. Paleostress reconstruction in the Tertiary basin areas in Southeastern Korea. Journal of the Korean Earth Science Society 21, 230–249 (in Korean with English abstract).
Oguchi, T., Ohmori, H., 1994. Analysis of relationships among alluvial fan area, source basin area, basin slope, and sediment yield. Zeitschrift für Geomorphologie 38, 405–420.
Oh, I.S., Jeong, G.S., 1975. The Geological Map of Gi Gae Sheet (1:50,000) and Explanatory Text. Geological and Mineral Institute of Korea 25 pp (in Korean and English abstract).
Olivarius, M., Rasmussen, E.S., Siersma, V., Knudsen, C., Kokfelt, T.F., Keulen, N., 2014. Provenance signal variations caused by facies and tectonics: zircon age and heavy mineral evidence from Miocene sand in the north-eastern North Sea Basin. Marine and Petroleum Geology 49, 1–14.
Paik, I.S., Lee, Y.I., Kim, H.J., Huh, M., 2012. Time, space and structure on the Korea Cretaceous dinosaur coast: Cretaceous stratigraphy, geochronology, and paleoenvironments. Ichnos 19, 6–16.
Park, M.E., Cho, H., Son, M., Sohn, Y.K., 2013. Depositional processes, paleoflow patterns, and evolution of a Miocene gravelly fan-delta system in SE Korea constrained by anisotropy of magnetic susceptibility analysis of interbedded mudrocks. Marine and Petroleum Geology 48, 206–223.
Paton, C., Woodhead, J.D., Hellstrom, J.C., Hergt, J.M., Greig, A., Maas, R., 2010. Improved laser ablation U-Pb zircon geochronology through robust downhole fractionation correction. Geochemistry, Geophysics, Geosystems 11, Q0AA06.
Paton, C., Hellstrom, J., Paul, B., Woodhead, J., Hergt, J., 2011. Iolite: freeware for the visualisation and processing of mass spectrometric data. Journal of Analytical Atomic Spectrometry 26, 2508–2518.
Petrus, J.A., Kamber, B.S., 2012. VizualAge: a novel approach to laser ablation ICP-MS U-Pb geochronology data reduction. Geostandards and Geoanalytical Research 36, 247–270.
Plyusnina, E.E., Ruban, D.A., Conrad, C.P., dos Anjos Zerfass, G.D.S., Zerfass, H., 2016. Long-term eustatic cyclicity in the Paleogene: a critical assessment. Proceedings of the Geologists' Association 127, 425–434.
Posamentier, H.W., Allen, G.P., 1993. Variability of the sequence stratigraphic model: effects of local basin factors. Sedimentary Geology 86, 91–109.
Ruban, D.A., 2016. A "chaos" of Phanerozoic eustatic curves. Journal of African Earth Sciences 116, 225–232.
Shin, S.-C., 2013. Revised fission-track ages and chronostratigraphies of the Miocene basin-fill volcanics and basements, SE Korea. Journal of the Petrological Society of Korea 22, 83–115 (in Korean with English abstract).
Sohn, Y.K., Son, M., 2004. Synrift stratigraphic geometry in a transfer zone coarse-grained delta complex, Miocene Pohang Basin, SE Korea. Sedimentology 51, 1387–1408.
Sohn, Y.K., Kim, S.B., Hwang, I.G., Bahk, J.J., Choe, M.Y., Chough, S.K., 1997. Characteristics and depositional processes of large-scale gravelly Gilbert-type foresets in the Miocene Doumsan fan delta, Pohang Basin, SE Korea. Journal of Sedimentary Research 67, 130–141.
Sohn, Y.K., Rhee, C.W., Shon, H., 2001. Revised stratigraphy and reinterpretation of the Miocene Pohang basinfill, SE Korea: sequence development in response to tectonism and eustasy in a back-arc basin margin. Sedimentary Geology 143, 265–285.
Son, M., Song, C.W., Kim, M.-C., Cheon, Y., Jung, S., Cho, H., Kim, H.-G., Kim, J.S., Sohn, Y.K., 2013. Miocene crustal deformation, basin development, and tectonic implication in the Southeastern Korean Peninsula. Journal of the Geological Society of Korea 49, 93–118 (in Korean with English abstract).
Son, M., Song, C.W., Kim, M.C., Cheon, Y., Cho, H., Sohn, Y.K., 2015. Miocene tectonic evolution of the basins and fault systems, SE Korea: dextral, simple shear during the East Sea (Sea of Japan) opening. Journal of the Geological Society 172, 664–680 (in Korean with English abstract).

Steiger, R.H., Jäger, E., 1977. Subcommission on geochronology: convention on the use of decay constants in geo- and cosmochronology. Earth and Planetary Science Letters 36, 359–362.
Talling, P.J., Stewart, M.D., Stark, C.P., Gupta, S., Vincent, S.J., 1997. Regular spacing of drainage outlets from linear fault blocks. Basin Research 9, 275–302.
Taylor, S.R., McLennan, S.M., 1985. The Continental Crust: Its Composition and Evolution. Blackwell Scientific Publications, Oxford, 315 pp.
Tucker, G.E., Whipple, K.X., 2002. Topographic outcomes predicted by stream erosion models: Sensitivity analysis and intermodel comparison. Journal of Geophysical Research 107 (B9), 2179.
Um, S.H., Lee, D.W., Bak, B.S., 1964 . The Geological Map of Pohang Sheet (1:50,000) and Explanatory Text. 25 pp (in Korean with English abstract).
Varva, G., Schmid, R., Gebauer, D., 1999. Internal morphology, habit and U-Th-Pb micro-analysis of amphibole to granulite facies zircon: geochronology of the Ivren Zone (Southern Alps). Contributions to Mineralogy and Petrology 134, 380–404.
Vermeesch, P., 2013. Multi-sample comparison of detrital age distributions. Chemical Geology 341, 140–146.
Wan, S., Kürschner, W.M., Clift, P.D., Li, A., Li, T., 2009. Extreme weathering/erosion during the Miocene Climatic Optimum: evidence from sediment record in the South China Sea. Geophysical Research Letters 36, L19706.
Wei, G., Li, X.-H., Liu, Y., Shao, L., Liang, X., 2006. Geochemical record of chemical weathering and monsoon climate change since the early Miocene in the South China Sea. Paleoceanography 21, PA4214.
Whipple, K.X., Trayler, C.R., 1996. Tectonic control of fan size: the importance of spatially variable subsidence rates. Basin Research 8, 351–366.
Whittaker, A.C., Attal, M.I., Allen, P.A., 2009. Characterising the origin, nature and fate of sediment exported from catchments perturbed by active tectonics. Basin Research 22, 809–828.
Wiedenbeck, M., AllÉ, P., Corfu, F., Griffin, W.L., Meier, M., Oberli, F., Quadt, A.V., Roddick, J.C., Spiegel, W., 1995. Three natural zircon standards for U-Th-Pb, Lu-Hf, trace element and REE analyses. Geostandards Newsletter 19, 1–23.
Yi, S., Yun, H., 1995. Miocene calcareous nannoplankton from the Pohang Basin, Korea. Palaeontographica (B) 237, 113–158.
Yoon, S.H., Chough, S.K., 1995. Regional strike slip in the eastern continental margin of Korea and its tectonic implications for the evolution of Ulleung Basin, East Sea (Sea of Japan). Geological Society of America Bulletin 107, 83–97.
You, Y., Huber, M., Müller, R.D., Poulsen, C.J., Ribbe, J., 2009. Simulation of the Middle Miocene Climate Optimum. Geophysical Research Letters 36, L04702.
Zachos, J., Pagani, M., Sloan, L., Thomas, E., Billups, K., 2001. Trends, rhythms, and aberrations in global climate 65 Ma to present. Science 292, 686–693.
Zhang, Y.-B., Zhai, M., Hou, Q.-L., Li, T.-S., Liu, F., Hu, B., 2012. Late Cretaceous volcanic rocks and associated granites in Gyeongsang Basin, SE Korea: their chronological ages and tectonic implications for cratonic destruction of the North China Craton. Journal of Asian Earth Sciences 47, 252–264.